SCIENTIFIC REPORTS

OPEN

Theoretical investigations on radiation generation of TEM, linearly or circularly polarized TE_{n1} coaxial waveguide mode in relativistic magnetron

Received: 6 December 2016
Accepted: 3 April 2017
Published online: 04 May 2017

Di-Fu Shi, Bao-Liang Qian, Hong-Gang Wang, Wei Li & Guang-Xing Du

The physical mechanism of the radiation generation of all possible output modes of the relativistic magnetron (RM) with all cavity-magnetron axial extraction technique is theoretically analysed, and the necessary conditions for generating these modes are obtained respectively. Assuming that n_0 is the number of the electron spokes, $N \geq 4$ as the total number of the cavities is an even number, and k is a nonnegative integer, some conclusions can be drawn as follows. If $n_0 = kN$ is true, no mode can be excited in the coaxial waveguide; if $n_0 = (2k+1)N/4$ is true, the linearly polarized modes can be excited in the coaxial waveguide; if $n_0 = (4k+2)N/4$ is true, the TEM mode and the linearly polarized modes can be excited in the coaxial waveguide; if n_0 takes other value, the left and right circularly polarized modes can be excited in the coaxial waveguide and the directions of rotation of the circularly polarized modes can be reversed with the reversion of the direction of rotation of the electron spokes; in addition, some other regular characteristics of the corresponding mode excitation are presented in detail in this paper. Such unique attractive properties that have been verified by the cold and hot simulations in this paper make it possible for this type of RM to meet application requirements of various high power microwave (HPM) modes.

Compared with linearly polarized microwaves, circularly polarized microwaves have been widely used in radar, navigation, guidance, communications, television broadcasts systems and so on, because most antennas that have different polarization directions can always receive circularly polarized microwaves. At present, high power microwave (HPM) sources of various types of structure and principle can generate microwaves with different modes in the output waveguide. However, except for the relativistic magnetron (RM), HPM sources that can generate circularly polarized microwaves without using mode converters are rarely reported. In fact, RMs can generate separately various microwave modes, such as a TE_{01} mode[1,2], a linearly polarized TE_{n1} ($n \geq 1$ is an integer) mode[1–5], or a circularly polarized TE_{n1} ($n \geq 2$ is an integer) mode[4–7] in circular waveguide, or a TE_{10} mode in rectangular waveguide[8,9]. Until 2012, RMs with all cavity-magnetron axial extraction technique were investigated with numerical simulation[10] and it has become possible to generate TEM modes in a coaxial waveguide. Then based on this technique, in 2016 a compact RM with the circularly polarized TE_{11} mode in a coaxial waveguide was proposed and verified by theoretical and simulation investigations[11]. And due to the uniqueness of the output mode, the RM seems more attractive and competitive than other HPM sources. However, comprehensively and thoroughly theoretical investigations on the radiation generation of all possible output modes of the RM with all cavity-magnetron axial extraction technique have not yet appeared in relevant literature.

In this paper, based on vector Helmholtz equation and field matching method, we have systematically analysed the physical mechanism of the radiation generation of all possible output modes of the RM with all cavity-magnetron axial extraction technique and have respectively obtained the necessary conditions for

College of Optoelectric Science and Engineering, National University of Defense Technology, Changsha, Hunan, 410073, People's Republic of China. Correspondence and requests for materials should be addressed to D.-F.S. (email: shidifu119@aliyun.com) or H.-G.W. (email: hg_wang11@sina.com)

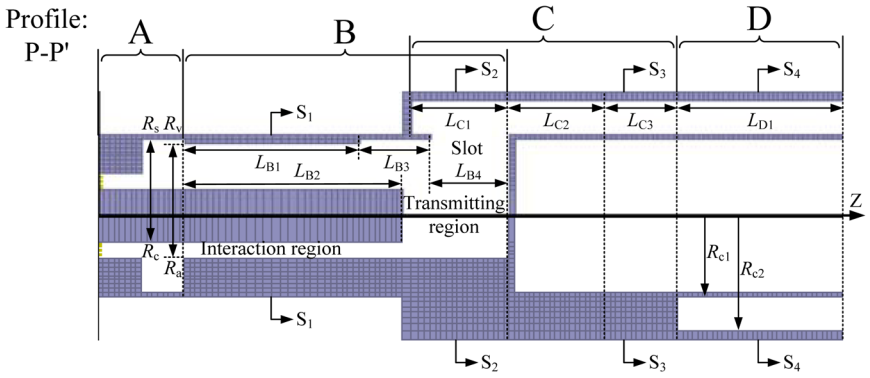

Figure 1. Schematic diagram of the longitudinal profile of the RM.

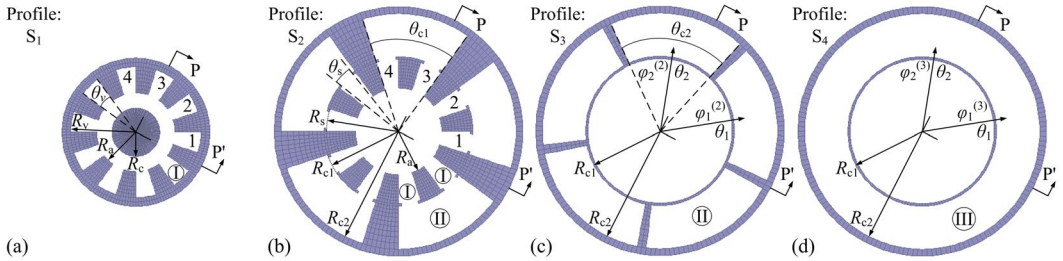

Figure 2. Schematic diagram of the transversal profiles of the RM in the (**a**) S_1 plane, (**b**) S_2 plane, (**c**) S_3 plane, and (**d**) S_4 plane.

generating TEM mode, linearly polarized TE_{n1} mode, and circularly polarized TE_{n1} mode in coaxial waveguide of the RM. Furthermore, the correctness of the theoretical analysis has been verified by the cold and hot simulations.

Theoretical analysis of mode excitation

Without loss of generality, a ten-cavity RM with all cavity-magnetron axial extraction technique, as was discussed in ref. 11, is taken into consideration. The longitudinal profile of the RM and the transversal profiles of the RM in the planes of S_1, S_2, S_3, and S_4 are shown in Figs 1 and 2 respectively. The whole structure of the RM is divided into four sections, namely section A of the coaxial waveguide for electric power input, section B of the resonant system for beam-wave interaction, section C of the sectorial waveguides arranged in an annulus for microwave extraction, and section D of the coaxial waveguide for microwave output. In the model, a resonant system with ten sector-type cavities is adopted. In the axial direction, L_{B1} indicates the length of the beam-wave interaction region; L_{B2} indicates the length of the cathode; L_{B4} indicates the length of the coupling slots; L_{B3} indicates the distance between the interaction region and the coupling slots; L_{C1} indicates the length of the anterior segment of the sectorial waveguides; L_{C2} indicates the length of the transition segment of the sectorial waveguides; L_{C3} indicates the length of the posterior segment of the sectorial waveguides; L_{D1} indicates the length of the coaxial waveguide in section D. In the transverse direction, R_c indicates the cathode radius; R_a indicates the anode radius; R_v indicates the cavity radius in the interaction region; R_s indicates the cavity radius in the transmitting region; R_{c1} indicates the inner radius of the sectorial waveguides; R_{c2} indicates the outer radius of the sectorial waveguides; θ_v indicates the cavity angle; θ_s indicates the coupling slot angle; θ_{c1} indicates the angle of the anterior segment of the sectorial waveguides; θ_{c2} indicates the angle of the posterior segment of the sectorial waveguides.

For the sake of convenient narration in the theoretical analysis, the cylindrical-coordinate system is established at the center of the RM; the observation in this paper is along the -Z direction; the cavities in section B are respectively numbered $p = 1, \ldots\ldots, N$ in a counterclockwise direction, where the total number of the cavities N is an even number equal to or greater than 4; the area in which RF fields exist is divided into three parts: area I of the cavities ($R_a < r < R_s$) with the longitudinal range of $L_{B1} + L_{B3} + L_{B4}$ in section B, area II of the sectorial waveguide ($R_{c1} < r < R_{c2}$) with the longitudinal range of $L_{C1} + L_{C2} + L_{C3}$ in section C, and area III of the coaxial waveguide ($R_{c1} < r < R_{c2}$) with the longitudinal range of L_{D1} in section D. In addition, all the theoretical analysis below is based on the premise that only the TE_{11} mode can propagate steadily in the sectorial waveguides of section C. Under the premise, the reflected waves with other waveguide modes in section C can not be excited yet. Thus, the reflected waves can not affect the output mode components in the coaxial waveguide of section D, and only the waves in the +Z direction are discussed here.

Analysis for area I. In area I, as the cavities with sectorial type are adopted, the axial component of magnetic field $H_z^{(1)}(r, \theta, z)$ in a sectorial cavity can be written as

$$H_z^{(1)}(r,\theta,z) = H_{z0}^{(1)}\left[N_{\nu_1}'(k_{c1}R_s)J_{\nu_1}(k_{c1}r) - J_{\nu_1}'(k_{c1}R_s)N_{\nu_1}(k_{c1}r)\right]\cos(\nu_1\theta)e^{-j\beta_1 z}, \tag{1}$$

where $H_{z0}^{(1)}$ is a constant, $\nu_1 = n_1\pi/\theta_v$, n_1 as the azimuthal mode number is a positive integer, $J_{\nu 1}(k_{c1}r)$ and $N_{\nu 1}(k_{c1}r)$ are the well-known Bessel and Neumann functions of order ν_1 respectively, k_{c1} is the transverse cutoff wave number, and β_1 is the axial propagation constant. A previous study has shown that the lowest azimuthal mode in the cavities dominants the beam-wave interaction of a RM[12], therefore $n_1 = 0$ and with Eq. (1) the azimuthal component of electric field in a sectorial cavity can be obtained as

$$E_\theta^{(1)}(r,\theta,z) = \frac{j\omega\mu}{k_{c1}}\frac{\partial H_z^{(1)}(r,\theta,z)}{\partial r} = E_\theta^{(1)}(r)e^{-j\beta_1 z}, \tag{2}$$

where $E_\theta^{(1)}(r)$ can be given as

$$E_\theta^{(1)}(r) = \frac{j\omega\mu}{k_{c1}}H_{z0}^{(1)}[N_0'(k_{c1}R_s)J_0'(k_{c1}r) - J_0'(k_{c1}R_s)N_0'(k_{c1}r)]. \tag{3}$$

Due to the periodically azimuthal symmetry of the cavities, the electromagnetic fields in the cavities have the same amplitude but with different phases. The phase difference between two adjacent cavities is $2\pi n_0/N$, where n_0 representing the number of the electron spokes indicates the azimuthal periodicity of the electromagnetic field distribution. Thus, with Eq. (2) the azimuthal component of electric field in a cavity can be expressed as

$$E_{\theta,p}^{(1)}(r,\theta,z) = E_\theta^{(1)}(r,\theta,z)e^{\pm j2\pi n_0 p/N}, \tag{4}$$

where "−" and "+" indicate the electron spokes rotate counterclockwise and clockwise respectively.

Without loss of generality the azimuthal components of the electric fields in the first four adjacent cavities which correspond to the first two adjacent sectorial waveguides are taken into consideration and with Eq. (4) they can be respectively given as

$$\begin{cases} E_{\theta,1}^{(1)}(r,\theta,z) = E_\theta^{(1)}(r,\theta,z)e^{\pm j2\pi n_0\cdot 1/N}, \\ E_{\theta,2}^{(1)}(r,\theta,z) = E_\theta^{(1)}(r,\theta,z)e^{\pm j2\pi n_0\cdot 2/N}, \\ E_{\theta,3}^{(1)}(r,\theta,z) = E_\theta^{(1)}(r,\theta,z)e^{\pm j2\pi n_0\cdot 3/N}, \\ E_{\theta,4}^{(1)}(r,\theta,z) = E_\theta^{(1)}(r,\theta,z)e^{\pm j2\pi n_0\cdot 4/N}. \end{cases} \tag{5}$$

Analysis for area II. In area II, the axial component of magnetic field $H_z^{(2)}(r,\theta,z)$ in a sectorial waveguide can be written as

$$H_z^{(2)}(r,\theta,z) = H_{z0}^{(2)}\left[N_{\nu_2}'(k_{c2}R_{c2})J_{\nu_2}(k_{c2}r) - J_{\nu_2}'(k_{c2}R_{c2})N_{\nu_2}(k_{c2}r)\right]\cos(\nu_2\theta)e^{-j\beta_2 z}, \tag{6}$$

where $H_{z0}^{(2)}$ is a constant, $\nu_2 = n_2\pi/\theta_{c2}$, n_2 as the azimuthal mode number is a positive integer, $J_{\nu 2}(k_{c2}r)$ and $N_{\nu 2}(k_{c2}r)$ are the well-known Bessel and Neumann functions of order ν_2 respectively, k_{c2} is the transverse cutoff wave number, and β_2 is the axial propagation constant. Since only the TE_{11} mode can propagate steadily in the sectorial waveguides, $n_2 = 1$ and with Eq. (6) the radial component of electric field in a sectorial waveguide can be obtained as

$$E_r^{(2)}(r,\theta,z) = -\frac{j\omega\mu}{k_{c2}^2 r}\frac{\partial H_z^{(2)}(r,\theta,z)}{\partial\theta} = E_r^{(2)}(r)\sin(\nu_2\theta)e^{-j\beta_2 z}, \tag{7}$$

where $E_r^{(2)}(\mathrm{r})$ can be given as

$$E_r^{(2)}(r) = \frac{j\omega\mu\nu_2}{k_{c2}^2 r}H_{z0}^{(2)}\left[N_{\nu_2}'(k_{c2}R_{c2})J_{\nu_2}(k_{c2}r) - J_{\nu_2}'(k_{c2}R_{c2})N_{\nu_2}(k_{c2}r)\right]. \tag{8}$$

Due to the bilateral symmetry between the extraction structures of the odd and even cavities in section C, all the amplitudes of the electric fields can vary from $E_\theta^{(1)}(r,\theta,z)$ in the cavities to $E_r^{(2)}(r,\theta,z)$ in the sectorial waveguides with the same variation, while the corresponding phase variations of the electric fields have some difference. Assuming that the phase variations of the electric fields from the odd cavities are $e^{j\alpha}$, the phase variations of the electric fields from the even cavities would be $e^{j\alpha}e^{j\pi}$. And with Eqs (5) and (7) the radial components of the electric fields in the first two sectorial waveguides extracted from the first four adjacent cavities can be respectively obtained as

$$\begin{cases} E_{r,1}^{(2)}(r,\theta_1,z) = E_r^{(2)}(r,\theta_1,z)e^{\pm j2\pi n_0\cdot 1/N}e^{j\alpha}, \\ E_{r,2}^{(2)}(r,\theta_1,z) = E_r^{(2)}(r,\theta_1,z)e^{\pm j2\pi n_0\cdot 2/N}e^{j\alpha}e^{j\pi}, \\ E_{r,3}^{(2)}(r,\theta_2,z) = E_r^{(2)}(r,\theta_2,z)e^{\pm j2\pi n_0\cdot 3/N}e^{j\alpha}, \\ E_{r,4}^{(2)}(r,\theta_2,z) = E_r^{(2)}(r,\theta_2,z)e^{\pm j2\pi n_0\cdot 4/N}e^{j\alpha}e^{j\pi}, \end{cases} \tag{9}$$

where θ_1 and θ_2 are the angular coordinates of the first two sectorial waveguides respectively, corresponding to the phases of $\varphi_1^{(2)}$ and $\varphi_2^{(2)}$.

For $n_0 = kN$, where k is a nonnegative integer, with Eq. (9) the radial components of the total electric fields in the first two sectorial waveguides are both equal to zero as shown in Eq. (10), as well as in other sectorial waveguides of section C.

$$E_{r,1}^{(2)}(r,\theta_1,z) + E_{r,2}^{(2)}(r,\theta_1,z) = E_{r,3}^{(2)}(r,\theta_2,z) + E_{r,4}^{(2)}(r,\theta_2,z) = 0. \tag{10}$$

Therefore, no waveguide mode will be excited in the sectorial waveguides, neither in the coaxial waveguide of section D.

For $n_0 \neq kN$, with Eq. (9) the phase difference $\Delta\varphi^{(2)} = \varphi_2^{(2)} - \varphi_1^{(2)}$ between the radial components of the total electric fields in the first two sectorial waveguides can be obtained as shown in Eq. (11), as well as in other two adjacent sectorial waveguides of section C.

$$\frac{E_{r,3}^{(2)}(r,\theta_2,z) + E_{r,4}^{(2)}(r,\theta_2,z)}{E_{r,1}^{(2)}(r,\theta_1,z) + E_{r,2}^{(2)}(r,\theta_1,z)} = e^{\pm j4\pi n_0/N} = e^{j\Delta\varphi^{(2)}}. \tag{11}$$

Analysis for area III. In area III, for TEM mode, the radial component of electric field in the coaxial waveguide can be written as

$$E_{r,\mathrm{TEM}}^{(3)}(r,z) = E_{r,\mathrm{TEM}}^{(3)}(r)e^{-jk_{\mathrm{TEM}}z}, \tag{12}$$

where $E_{r,\mathrm{TEM}}^{(3)}(r) = E_0/r$, E_0 is a constant, and k_{TEM} is the transverse cutoff wave number.

For TE_{n1} mode, assuming that the axial component of magnetic field $H_{z,\mathrm{TE}}^{(3)}(r,\theta,z)$ in the coaxial waveguide is an even function about $\theta = 0$ without loss of generality, one can get

$$H_{z,\mathrm{TE}}^{(3)}(r,\theta,z) = H_{z0,n_3}^{(3)}\left[N_{n_3}'\left(k_{c3,n_3}R_{c2}\right)J_{n_3}\left(k_{c3,n_3}r\right) - J_{n_3}'\left(k_{c3,n_3}R_{c2}\right)N_{n_3}\left(k_{c3,n_3}r\right)\right]\cos(n_3\theta) e^{-j\beta_{3,n_3}z}, \tag{13}$$

where $H_{z0,n3}^{(3)}$ is a constant, n_3 as the azimuthal mode number is a positive integer, $J_{n3}(k_{c3,n3}r)$ and $N_{n3}(k_{c3,n3}r)$ are the well-known Bessel and Neumann functions of order n_3 respectively, $k_{c3,n3}$ is the transverse cutoff wave number, and $\beta_{3,n3}$ is the axial propagation constant. With Eq. (13) the radial component of electric field in the coaxial waveguide can be obtained as

$$E_{r,\mathrm{TE}}^{(3)}(r,\theta,z) = -\frac{j\omega\mu}{k_{c3,n_3}^2 r}\frac{\partial H_{z,\mathrm{TE}}^{(3)}(r,\theta,z)}{\partial\theta} = E_{r,\mathrm{TE}}^{(3)}(r)\sin(n_3\theta)e^{-j\beta_{3,n_3}z}, \tag{14}$$

where $E_{r,\mathrm{TE}}^{(3)}(r)$ can be given as

$$E_{r,\mathrm{TE}}^{(3)}(r) = \frac{j\omega\mu n_3}{k_{c3,n_3}^2 r}H_{z0,n_3}^{(3)}\left[N_{n_3}'\left(k_{c3,n_3}R_{c2}\right)J_{n_3}\left(k_{c3,n_3}r\right) - J_{n_3}'\left(k_{c3,n_3}R_{c2}\right)N_{n_3}\left(k_{c3,n_3}r\right)\right]. \tag{15}$$

In order to construct an electromagnetic field function of a circularly polarized coaxial waveguide mode, the radial components of electric fields of two polarized degenerate modes with an angular phase difference of $\pi/2$ are required.

For left circular polarization, with Eq. (14) the radial components of electric fields of two polarized degenerate modes can be written as

$$\begin{cases} E_{r,\mathrm{TE},L1}^{(3)}(r,\theta,z) = E_{r,\mathrm{TE},L}^{(3)}(r)\sin(n_L\theta)e^{-j\beta_{3,n_L}z}, \\ E_{r,\mathrm{TE},L2}^{(3)}(r,\theta,z) = E_{r,\mathrm{TE},L}^{(3)}(r)\sin\left(n_L\theta - \frac{\pi}{2}\right)e^{-j\pi/2}e^{-j\beta_{3,n_L}z}, \end{cases} \tag{16}$$

where n_L is used instead of n_3. With Eq. (16) the radial component of total electric field of the left circularly polarized coaxial waveguide mode can be obtained as

$$E_{r,\mathrm{TE},L}^{(3)}(r,\theta,z) = E_{r,\mathrm{TE},L1}^{(3)}(r,\theta,z) + E_{r,\mathrm{TE},L2}^{(3)}(r,\theta,z) = E_{r,\mathrm{TE},L}^{(3)}(r)e^{j(\pi/2-n_L\theta)}e^{-j\beta_{3,n_L}z}. \tag{17}$$

For right circular polarization, with Eq. (14) the radial components of electric fields of two polarized degenerate modes can be written as

$$\begin{cases} E^{(3)}_{r,\mathrm{TE},R1}(r,\theta,z) = E^{(3)}_{r,\mathrm{TE},R}(r)\sin(n_R\theta)e^{-j\beta_{3,n_R}z}, \\ E^{(3)}_{r,\mathrm{TE},R2}(r,\theta,z) = E^{(3)}_{r,\mathrm{TE},R}(r)\sin\left(n_R\theta - \frac{\pi}{2}\right)e^{j\pi/2}e^{-j\beta_{3,n_R}z}, \end{cases} \tag{18}$$

where n_R is used instead of n_3. With Eq. (18) the radial component of total electric field of the right circularly polarized coaxial waveguide mode can be obtained as

$$E^{(3)}_{r,\mathrm{TE},R}(r,\theta,z) = E^{(3)}_{r,\mathrm{TE},R1}(r,\theta,z) + E^{(3)}_{r,\mathrm{TE},R2}(r,\theta,z) = E^{(3)}_{r,\mathrm{TE},R}(r)e^{j(n_R\theta-\pi/2)}e^{-j\beta_{3,n_R}z}. \tag{19}$$

Solutions for matched fields. The electric fields of area II and area III should be matched on the boundary of the two areas. With Eqs (12), (17) and (19) the phase difference $\Delta\varphi^{(3)} = \varphi_2{}^{(3)} - \varphi_1{}^{(3)}$ between the radial components of the total electric fields with the angle difference of $\Delta\theta = \theta_2 - \theta_1 = 4\pi/N$ in the coaxial waveguide should be equal to the phase difference $\Delta\varphi^{(2)}$ between the radial components of the total electric fields in the first two sectorial waveguides in Eq. (11), as shown in Eq. (20).

$$\frac{E^{(3)}_{r,\mathrm{TEM}}(r,z) + \sum_{n_L=1}^{\infty}E^{(3)}_{r,\mathrm{TE},L}(r,\theta_2,z) + \sum_{n_R=1}^{\infty}E^{(3)}_{r,\mathrm{TE},R}(r,\theta_2,z)}{E^{(3)}_{r,\mathrm{TEM}}(r,z) + \sum_{n_L=1}^{\infty}E^{(3)}_{r,\mathrm{TE},L}(r,\theta_1,z) + \sum_{n_R=1}^{\infty}E^{(3)}_{r,\mathrm{TE},R}(r,\theta_1,z)} = e^{j\Delta\varphi^{(3)}} = e^{j\Delta\varphi^{(2)}} = e^{\pm j4\pi n_0/N}, \tag{20}$$

where θ_1 and θ_2 are the angular coordinates of the first two sectorial waveguides respectively, corresponding to the phases of $\varphi_1{}^{(3)}$ and $\varphi_2{}^{(3)}$. Thus,

$$\begin{aligned} &E^{(3)}_{r,\mathrm{TEM}}(r)[1 - e^{\pm j4\pi n_0/N}]e^{-jk_{\mathrm{TEM}}z} \\ &+ \sum_{n_L=1}^{\infty}E^{(3)}_{r,\mathrm{TE},L}(r)[e^{j(\pi/2-n_L\theta_2)} - e^{j(\pi/2-n_L\theta_1)\pm j4\pi n_0/N}]e^{-j\beta_{3,n_L}z} \\ &+ \sum_{n_R=1}^{\infty}E^{(3)}_{r,\mathrm{TE},R}(r)[e^{j(n_R\theta_2-\pi/2)} - e^{j(n_R\theta_1-\pi/2)\pm j4\pi n_0/N}]e^{-j\beta_{3,n_R}z} = 0. \end{aligned} \tag{21}$$

Taking $n_0 \neq kN$ and general phase difference into consideration, the solutions of Eq. (21) can be described as follows.

For the counterclockwise rotation of electron spokes where "±" takes the minus, the solutions of generating the TEM mode, the left and right circularly polarized $\mathrm{TE_{n1}}$ coaxial waveguide modes can be respectively obtained as

$$\begin{cases} n_0 = \frac{N}{2}(2k+1), \quad k \in Z \text{ and } k \geq 0, \\ n_L = n_0 - \frac{N}{2}p_L, \quad p_L \in Z \text{ and } p_L < \frac{2n_0}{N}, \\ n_R = -n_0 + \frac{N}{2}p_R, \quad p_R \in Z \text{ and } p_R > \frac{2n_0}{N}. \end{cases} \tag{22}$$

where Z is the set of all integers.

For the clockwise rotation of electron spokes where "±" takes the plus, the solutions of generating the TEM mode, the left and right circularly polarized $\mathrm{TE_{n1}}$ coaxial waveguide modes can be respectively obtained as

$$\begin{cases} n_0 = \frac{N}{2}(2k+1), \quad k \in Z \text{ and } k \geq 0, \\ n_L = -n_0 - \frac{N}{2}q_L, \quad q_L \in Z \text{ and } q_L < -\frac{2n_0}{N}, \\ n_R = n_0 + \frac{N}{2}q_R, \quad q_R \in Z \text{ and } q_R > -\frac{2n_0}{N}. \end{cases} \tag{23}$$

where Z is the set of all integers.

According to Eqs (22) and (23), the necessary condition for $n_L = n_R$ is $n_0 = (2k+1)N/4$ or $n_0 = (4k+2)N/4$ where k is a nonnegative integer, thus three cases have to be discussed as follows.

(1) Firstly, if $n_0 = (2k+1)N/4$ is true, Eq. (11) can be written as

$$\frac{E^{(2)}_{r,3}(r,\theta_2,z) + E^{(2)}_{r,4}(r,\theta_2,z)}{E^{(2)}_{r,1}(r,\theta_1,z) + E^{(2)}_{r,2}(r,\theta_1,z)} = -1. \tag{24}$$

It means that the electric fields in any two adjacent sectorial waveguides have the same amplitude but with a phase difference of 180°.

For the counterclockwise rotation of electron spokes, according to Eq. (22), the TEM mode can not be

excited.
For circularly polarized mode, since n_L and n_R from Eq. (22) can be rewritten as

$$\begin{cases} n_L = \frac{N}{4}[(2k+1) - 2p_L], & p_L \in Z \text{ and } p_L < \frac{1}{2}(2k+1), \\ n_R = \frac{N}{4}[2p_R - (2k+1)], & p_R \in Z \text{ and } p_R > \frac{1}{2}(2k+1), \end{cases} \tag{25}$$

they can be equivalent to the same arithmetic progression with the first term of $N/4$ and the common difference of $N/2$, as shown in Eq. (26).

$$n_L = n_R = \frac{N}{4} + t\frac{N}{2}, \quad t \in Z \text{ and } t \geq 0. \tag{26}$$

Thus, the left and right circularly polarized modes have the same set of azimuthal mode numbers of $(N/4 + tN/2)$ but with different directions of rotation, as a result that the linearly polarized modes consisting of the corresponding left and right circularly polarized modes can be excited, and the solutions of generating the linearly polarized modes for different values of n_0 are equivalent.
For the clockwise rotation of electron spokes, the same conclusion also can be obtained.

(2) Secondly, if $n_0 = (4k+2)N/4$ is true, Eq. (11) can be written as

$$\frac{E^{(2)}_{r,3}(r, \theta_2, z) + E^{(2)}_{r,4}(r, \theta_2, z)}{E^{(2)}_{r,1}(r, \theta_1, z) + E^{(2)}_{r,2}(r, \theta_1, z)} = 1 \tag{27}$$

It means that the electric fields in any two adjacent sectorial waveguides have the same amplitude and phase.
For the counterclockwise rotation of electron spokes, according to Eq. (22), the TEM mode can be excited.
For circularly polarized mode, since n_L and n_R from Eq. (22) can be rewritten as

$$\begin{cases} n_L = \frac{N}{2}[(2k+1) - p_L], & p_L \in Z \text{ and } p_L < 2k+1, \\ n_R = \frac{N}{2}[p_R - (2k+1)], & p_R \in Z \text{ and } p_R > 2k+1, \end{cases} \tag{28}$$

they can be equivalent to the same arithmetic progression with the first term of $N/2$ and the common difference of $N/2$, as shown in Eq. (29).

$$n_L = n_R = \frac{N}{2} + t\frac{N}{2}, \quad t \in Z \text{ and } t \geq 0. \tag{29}$$

Thus, the left and right circularly polarized modes have the same set of azimuthal mode numbers of $(N/2 + tN/2)$ but with different directions of rotation, as a result that the linearly polarized modes consisting of the corresponding left and right circularly polarized modes can be excited, and the solutions of generating the TEM mode and the linearly polarized modes for different values of n_0 are equivalent.
For the clockwise rotation of electron spokes, the same conclusion also can be obtained.

(3) Thirdly, if n_0 takes other values, $n_L \neq n_R$.

For the counterclockwise rotation of electron spokes, according to Eq. (22), the TEM mode can not be excited, while the left circularly polarized modes with the set of azimuthal mode numbers of $(n_0 - p_L N/2)$ and the right circularly polarized modes with the set of azimuthal mode numbers of $(-n_0 + p_R N/2)$ can be excited. Comparing the two cases of the numbers of the electron spokes of $n_0' = n_0 + s_1 N/2$ and n_0 where $s_1 > -2n_0/N$ is an integer, with Eq. (22) one can see that the solutions of generating the left and right circularly polarized modes for n_0' and n_0 are equivalent. Comparing the two cases of the numbers of the electron spokes of $n_0'' = -n_0 + s_2 N/2$ and n_0 where $s_2 > 2n_0/N$ is an integer, with Eq. (22) one can see that the solutions of generating the left and right circularly polarized modes for n_0'' are equivalent to the solutions of generating the right and left circularly polarized modes for n_0 respectively.

For the clockwise rotation of electron spokes, the similar conclusions also can be obtained.

In addition, comparing Eq. (22) with Eq. (23), one can see that the solutions of generating the left and right circularly polarized modes for the counterclockwise rotation of electron spokes are equivalent to the solutions of generating the right and left circularly polarized modes for the clockwise rotation of electron spokes respectively. It means that the directions of rotation of the circularly polarized modes can be reversed with the reversion of the direction of rotation of the electron spokes.

Summary. To sum up briefly, at least four conclusions, where k and t are nonnegative integers, can be drawn as follows.

(1) If $n_0 = kN$ is true, no mode can be excited in the coaxial waveguide.
(2) If $n_0 = (2k+1)N/4$ is true, the linearly polarized modes with the set of azimuthal mode numbers of $(N/4 + tN/2)$ can be excited in the coaxial waveguide, and the solutions of generating the linearly polarized

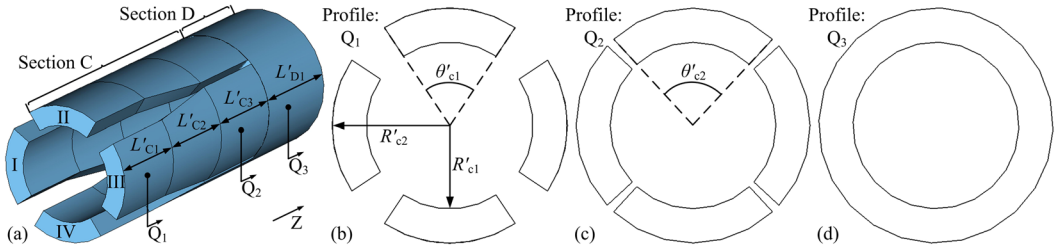

Figure 3. Schematic diagram of the (**a**) inner space of section C and D in an eight-cavity RM, and its transversal profiles in the (**b**) Q_1 plane, (**c**) Q_2 plane and (**d**) Q_3 plane.

Parameters	R'_{c1} (mm)	R'_{c2} (mm)	θ'_{c1} (°)	θ'_{c2} (°)	L'_{C1} (mm)	L'_{C2} (mm)	L'_{C3} (mm)	L'_{D1} (mm)
Values	34.0	48.0	67.5	85.5	60.0	60.0	60.0	70.0

Table 1. Structure parameters of section C and D in an eight-cavity RM.

n_0	0	1	2	3	4	5	6	7	8	12
n_L,1 ($TE_{nL,1}$)	/	1,1	2,1*	3,1	TEM** & 4,1*	1,1	2,1*	3,1	/	TEM** & 4,1*
η ($TE_{nL,1}$)	/	71.00%	99.95%	28.93%	91.53% & 8.33%	71.00%	99.95%	28.93%	/	91.53% & 8.33%
n_R,1 ($TE_{nR,1}$)	/	3,1	2,1*	1,1	TEM** & 4,1*	3,1	2,1*	1,1	/	TEM** & 4,1*
η ($TE_{nR,1}$)	/	28.93%	99.95%	71.01%	91.53% & 8.33%	28.93%	99.95%	71.01%	/	91.53% & 8.33%

Table 2. Output mode components of the eight-cavity RM with their corresponding proportions in the coaxial waveguide in the cold simulations. *$n_L = n_R$ indicates that the TE coaxial waveguide mode is linearly polarized, and the corresponding value of η is the simulation result for the linearly polarized mode. **The TEM mode is neither linearly polarized nor circularly polarized, and the corresponding value of η is the simulation result for the TEM mode.

modes for different values of n_0 are equivalent.

(3) If $n_0 = (4k+2)N/4$ is true, the TEM mode and the linearly polarized modes with the set of azimuthal mode numbers of $(N/2 + tN/2)$ can be excited in the coaxial waveguide, and the solutions of generating the TEM mode and the linearly polarized modes for different values of n_0 are equivalent.

(4) If n_0 takes other value, the left and right circularly polarized modes with their corresponding sets of azimuthal mode numbers can be excited in the coaxial waveguide. Comparing the two cases of the numbers of the electron spokes of $n_0' = n_0 + s_1N/2$ and n_0 where $s_1 > -2n_0/N$ is an integer, the solutions of generating the left and right circularly polarized modes for n_0' and n_0 are equivalent. Comparing the two cases of the numbers of the electron spokes of $n_0'' = -n_0 + s_2N/2$ and n_0 where $s_2 > 2n_0/N$ is an integer, the solutions of generating the left and right circularly polarized modes for n_0'' are equivalent to the solutions of generating the right and left circularly polarized modes for n_0 respectively. In addition, the directions of rotation of the circularly polarized modes can be reversed with the reversion of the direction of rotation of the electron spokes.

Cold simulation verification

To verify the correctness of the theoretical analysis in section 2 in cold simulations (electromagnetic microwave simulations without simulation particles), the structure of section C and D in an eight-cavity RM ($N = 8$) as a typical example is investigated by the software CST Studio Suite[13]. The schematic diagrams of the model are shown in Fig. 3, and the structure parameters of the model are shown in Table 1. It is easy to figure out that at a frequency of 4.8 GHz for instance, only the TE_{11} mode can propagate steadily in the sectorial waveguides of section C and only the TEM, TE_{11}, TE_{21}, TE_{31}, and TE_{41} modes can propagate steadily in the coaxial waveguide of section D, while other waveguide modes are evanescent higher order modes.

According to Eq. (11), for the counterclockwise rotation of electron spokes, the TE_{11} modes with the same amplitude and the initial phases of $3n_0\pi/2$, $2n_0\pi/2$, $n_0\pi/2$, and 0 at 4.8 GHz are fed into sectorial waveguides I~IV of section C respectively. Then the output mode components with their corresponding proportions can be obtained from the port of section D in the cold simulations as shown in Table 2. In Table 2, n_0 is 12 or a number from 1 to 7, η as mode conversion efficiency can be figured out by mode transmission coefficient obtained from simulation results, and the direction of rotation of the circularly polarized modes can be determined by the phase

Parameters	R_c (mm)	R_a (mm)	R_v (mm)	R_s (mm)	R_{c1} (mm)	R_{c2} (mm)	θ_v (°)	θ_s (°)	θ_{c1} (°)
Values	11.0	18.0	30.0	32.0	34.0	48.0	18.0	18.0	54.0
Parameters	θ_{c2} (°)	L_{B1} (mm)	L_{B2} (mm)	L_{B3} (mm)	L_{B4} (mm)	L_{C1} (mm)	L_{C2} (mm)	L_{C3} (mm)	L_{D1} (mm)
Values	67.5	72.0	90.0	30.0	32.5	40.5	40.0	30.0	70.0

Table 3. Structure parameters of the ten-cavity RM.

n_0	0	1	2	3	4	5	6	7	8	9	10
n_L,1 ($TE_{nL,1}$)	/	1,1	2,1	3,1	(4,1)*	TEM & (5,1)*	1,1	2,1	3,1	(4,1)*	/
n_R,1 ($TE_{nR,1}$)	/	(4,1)*	3,1	2,1	1,1	TEM & (5,1)*	(4,1)*	3,1	2,1	1,1	/

Table 4. Output mode components of the ten-cavity RM in the coaxial waveguide in the cold simulations *Indicates that the mode in the bracket is an evanescent higher order mode.

relationship between two polarized degenerate modes shown in simulations. In addition, no mode can be excited in the coaxial waveguide when n_0 is 0 or 8 according to Eq. (10).

From Table 2, one can see that for the eight-cavity RM ($N=8$) in the cold simulations when $n_0=2$ or 6, the linearly polarized TE_{21} mode can be excited in the coaxial waveguide, and the solutions of generating the linearly polarized mode for $n_0=2$ and 6 are equivalent; when $n_0=4$ or 12, the TEM mode and the linearly polarized TE_{41} mode can be excited in the coaxial waveguide, and the solutions of generating the TEM mode and the linearly polarized mode for $n_0=4$ and 12 are equivalent; when $n_0=1$ or 5, the left circularly polarized TE_{11} mode and the right circularly polarized TE_{31} mode can be excited in the coaxial waveguide, and the solutions of generating the left and right circularly polarized modes for $n_0=1$ and 5 are equivalent; when $n_0=3$ or 7, the left circularly polarized TE_{31} mode and the right circularly polarized TE_{11} mode can be excited in the coaxial waveguide, and the solutions of generating the left and right circularly polarized modes for $n_0=3$ and 7 are equivalent; comparing the two cases of $n_0=1$ and 3, the solutions of generating the left and right circularly polarized modes for $n_0=1$ are equivalent to the solutions of generating the right and left circularly polarized modes for $n_0=3$ respectively; comparing the two cases of $n_0=1$ and 7, $n_0=3$ and 5, or $n_0=5$ and 7, the similar conclusions also can be obtained; in addition, the directions of rotation of the circularly polarized modes can be reversed with the reversion of the direction of rotation of the electron spokes.

Obviously these cold simulation results are absolutely consistent with the theoretical analysis described in section 2. And for other cases of $n_0>8$ in this model and other models of $N\neq 8$, the theoretical analysis also can be proved correct by the cold simulations which may be not necessary to show here one by one.

Hot simulation verification

To further confirm the correctness of the theoretical analysis in section 2, the hot simulations (electromagnetic microwave simulations with simulation particles) are run for typical RM structures. In order to obtain a pure TEM or TE_{n1} mode with slight modifications of electrical parameters or structural parameters in the hot simulations without loss of generality, a ten-cavity RM ($N=10$) is investigated by using the CHIPIC software[14]. The initial structure of the RM model shown in Figs 1 and 2 with its structure parameters shown in Table 3 is predesigned for obtaining the TEM mode with five electron spokes. It is easy to figure out that at an operating frequency of 4.30 GHz only the TE_{11} mode can propagate steadily in the sectorial waveguides and only the TEM, TE_{11}, TE_{21}, and TE_{31} modes can propagate steadily in the coaxial waveguide, while other waveguide modes are evanescent higher-order modes. Since the user-specified direction of the applied axial magnetic field is along the +Z direction, the direction of rotation of electron spokes is considered counterclockwise according to the direction of $\boldsymbol{E}_r \times \boldsymbol{B}_z$, where $\boldsymbol{E}_r$ is the radial component of the applied electric field and $\boldsymbol{B}_z$ is the axial component of the applied magnetic field. Then, based on the theoretical analysis in section 2, with Eq. (22) the output mode components of the ten-cavity RM in the coaxial waveguide in the cold simulations can be given in Table 4.

TEM mode for $n_0=5$. For obtaining the TEM mode with five electron spokes ($n_0=5$), a voltage of 220 kV and an axial magnetic field of 0.4 T are applied to drive the RM on the CHIPIC software.

Figure 4(a) shows that five electron spokes in the ten-cavity RM have been completely formed in angular direction.

Figure 4(b) shows that the frequency $f=4.30$ GHz is the dominating operating frequency since its spectral amplitude is at least 47.268 dB higher than those of other frequencies.

Figure 4(c) shows that the output mode is the TEM mode, which is consistent with the theoretical analysis and the cold simulation.

Circularly polarized TE_{11} mode for $n_0=4$. For obtaining the circularly polarized TE_{11} mode with four electron spokes ($n_0=4$), a voltage of 280 kV and an axial magnetic field of 0.4 T are applied to drive the RM on the CHIPIC software, where the cathode radius $R_c=9$ mm is used for the present case.

Figure 5(a) shows that four electron spokes in the ten-cavity RM have been completely formed in angular direction.

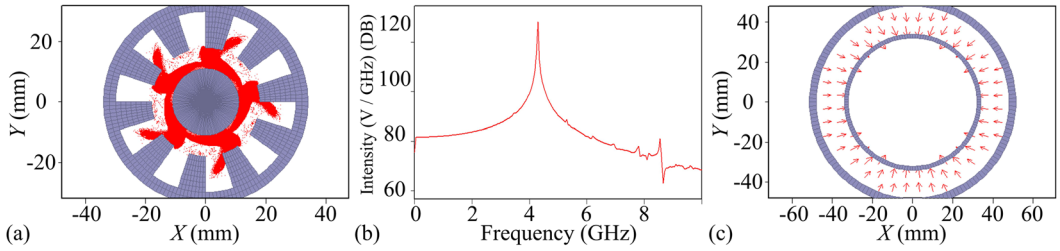

Figure 4. (**a**) Five electron spokes in the Rθ plane of the ten-cavity RM. (**b**) Spectrums of electric fields in dB in the output port of the coaxial waveguide from 20 to 40 ns. (**c**) TEM mode in the output port.

Figure 5(b) shows that the frequency $f = 4.20$ GHz is the dominating operating frequency since its spectral amplitude is at least 44.894 dB higher than those of other frequencies.

Figures 5(c,d) show the output mode patterns in the output port at $t = 27.949$ ns and 29.201 ns respectively. These are both the TE_{n1} mode ($n = 1$) but with different polarization directions and can be unambiguously identified as the circularly polarized TE_{11} mode. According to the time difference of the two TE_{11} modes ($\Delta t = 29.201 - 27.949 = 1.252$ ns), the period of rotation of the circularly polarized TE_{11} mode ($T_{TE11} = n/f = 1/4.2$ ns), and the angle difference of the polarization, one can easily figure out that the TE_{11} mode is right circularly polarized, which is consistent with the theoretical analysis and the cold simulation.

Circularly polarized TE_{11} mode for $n_0 = 6$. For obtaining the circularly polarized TE_{11} mode with six electron spokes ($n_0 = 6$), a voltage of 160 kV and an axial magnetic field of 0.4 T are applied to drive the RM on the CHIPIC software, where the cathode radius $R_c = 13$ mm is used for the present case.

Figure 6(a) shows that six electron spokes in the ten-cavity RM have been completely formed in angular direction.

Figure 6(b) shows that the frequency $f = 4.25$ GHz is the dominating operating frequency since its spectral amplitude is at least 17.6 dB higher than those of other frequencies.

Figure 6(c,d) shows the output mode patterns in the output port at $t = 29.323$ ns and 30.779 ns respectively. These patterns fall into the category of the TE_{n1} mode ($n = 1$) but with different polarization directions and they can be unambiguously identified as the circularly polarized TE_{11} mode. According to the time difference of the two TE_{11} modes ($\Delta t = 30.779 - 29.323 = 1.456$ ns), the period of rotation of the circularly polarized TE_{11} mode ($T_{TE11} = n/f = 1/4.25$ ns), and the angle difference of the polarization, one can easily figure out that the TE_{11} mode is left circularly polarized, which is consistent with the theoretical analysis and the cold simulation.

Circularly polarized TE_{21} mode for $n_0 = 3$. For obtaining the circularly polarized TE_{21} mode with three electron spokes ($n_0 = 3$), a voltage of 320 kV and an axial magnetic field of 0.4 T are applied to drive the RM on the CHIPIC software, where the cathode radius $R_c = 8$ mm is used for the present case.

Figure 7(a) shows that three electron spokes in the ten-cavity RM have been completely formed in angular direction.

Figure 7(b) shows that the frequency $f = 4.10$ GHz is the dominating operating frequency since its spectral amplitude is at least 30.614 dB higher than those of other frequencies.

However, as the theoretical analysis is given in section 2 and the output mode components of the ten-cavity RM in the coaxial waveguide in the cold simulations are shown in Table 4, both the TE_{21} and TE_{31} modes can be excited and propagate steadily in the coaxial waveguide, so that it is difficult to identify the output mode pattern shown in Fig. 7(c).

In order to suppress the TE_{31} mode component and obtain only the TE_{21} mode, a simple approach such as adjusting the radial dimensions of the coaxial waveguide may be feasible. As is shown in Fig. 8(a), the structure of section E consisting of a modified coaxial waveguide with the inner radius of 18.0 mm and the outer radius of 32.0 mm, and a tapered coaxial waveguide connecting the modified coaxial waveguide to the end of section C is used instead of the structure of section D.

Figure 8(b,c) show the output mode patterns in the output port of the modified RM at $t = 28.954$ ns and 29.996 ns respectively. These patterns fall into the category of the TE_{n1} mode ($n = 2$) but with different polarization directions and they can be unambiguously identified as the circularly polarized TE_{21} mode. According to the time difference of the two TE_{21} modes ($\Delta t = 29.996 - 28.954 = 1.042$ ns), the period of rotation of the circularly polarized TE_{21} mode ($T_{TE21} = n/f = 2/4.10$ ns), and the angle difference of the polarization, one can easily figure out that the TE_{21} mode is right circularly polarized, which is consistent with the theoretical analysis and the cold simulation.

In addition, from the hot simulations above, it is worth noting that the direction of rotation of the circularly polarized modes can be easily reversed with the reversion of the direction of rotation of the electron spokes by reversing the current of the magnetic coils, while the TEM mode and the linearly polarized modes are unaffected by the direction of rotation of the electron spokes.

Conclusion

In this paper, through theoretically analysing the physical mechanism of the radiation generation of all possible output modes of the RM with all cavity-magnetron axial extraction technique, the necessary conditions for

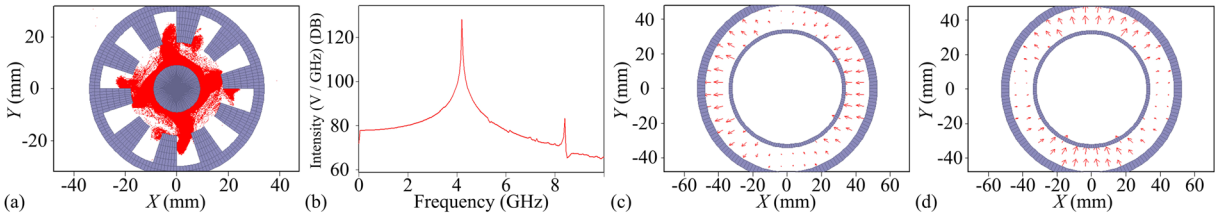

Figure 5. (**a**) Four electron spokes in the Rθ plane of the ten-cavity RM. (**b**) Spectrums of electric fields in dB in the output port of the coaxial waveguide from 20 to 40 ns. (**c**) TE_{11} mode in the output port at 27.949 ns. (**d**) TE_{11} mode in the output port at 29.201 ns.

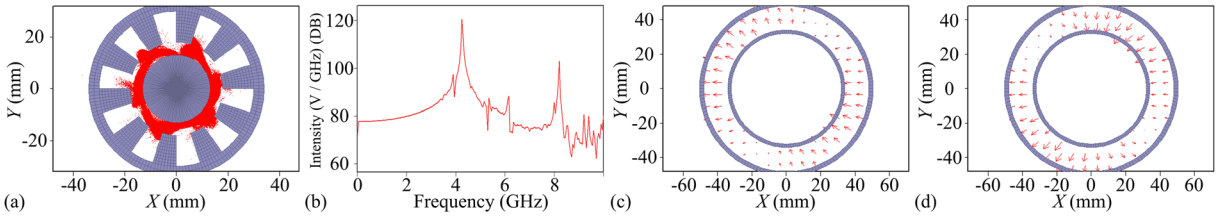

Figure 6. (**a**) Six electron spokes in the Rθ plane of the ten-cavity RM. (**b**) Spectrums of electric fields in dB in the output port of the coaxial waveguide from 20 to 40 ns. (**c**) TE_{11} mode in the output port at 29.323 ns. (**d**) TE_{11} mode in the output port at 30.779 ns.

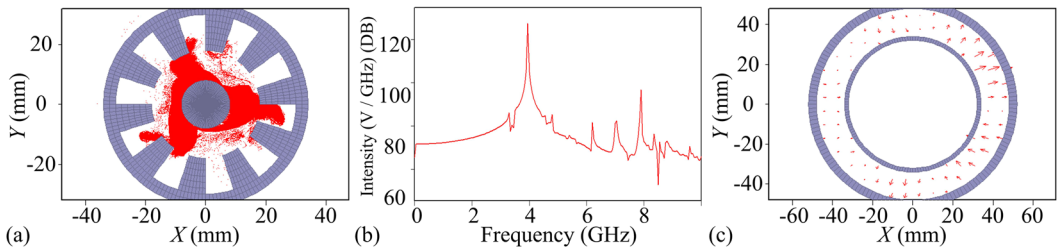

Figure 7. (**a**) Three electron spokes in the Rθ plane of the ten-cavity RM. (**b**) Spectrums of electric fields in dB in the output port of the coaxial waveguide from 20 to 40 ns. (**c**) Mixed modes in the output port.

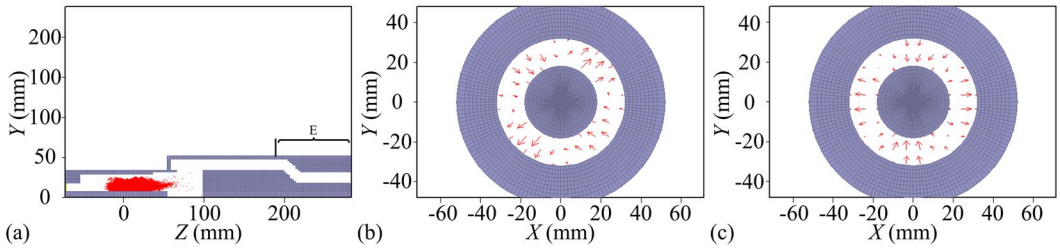

Figure 8. (**a**) Electron spokes in the RZ plane of the ten-cavity RM with section E replacing section D. (**b**) TE_{21} mode in the output port at 28.954 ns. (**c**) TE_{21} mode in the output port at 29.996 ns.

generating the TEM mode, the linearly polarized TE_{n1} mode, and the circularly polarized TE_{n1} mode in the coaxial waveguide are obtained respectively, as well as some regular characteristics of the corresponding mode excitation, and then verified by the cold and hot simulations. Undoubtedly, these theoretical investigations provide a comprehensively and thoroughly theoretical guidance for designing this type of RM. And more importantly, they not only show that the RM has the ability of generating any a mode among the TEM mode, the linearly polarized TE_{n1} mode, and the circularly polarized TE_{n1} mode in the coaxial waveguide, but also indicate that the direction of rotation of the circularly polarized mode can be easily reversed with the reversion of the direction of rotation of the electron spokes by reversing the current of the magnetic coils. Such unique attractive properties make it possible for this type of RM to meet application requirements of various HPM modes.

References

1. Fuks, M. I., Kovalev, N. F., Andreev, A. D. & Schamiloglu, E. Mode conversion in a magnetron with axial extraction of radiation. *IEEE Trans. Plasma Sci.* **34**, 620–626, doi:10.1109/TPS.2006.875770 (2006).
2. Li, W., Liu, Y.-G., Zhang, J., Shi, D.-F. & Zhang, W.-Q. Experimental investigations on the relations between configurations and radiation patterns of a relativistic magnetron with diffraction output. *J. Appl. Phys.* **113**, 023304, doi:10.1063/1.4774245 (2013).
3. Shi., D.-F., Qian, B.-L., Wang, H.-G. & Li, W. A novel TE_{11} mode axial output structure for a compact relativistic magnetron. *J. Phys. D: Appl. Phys.* **49**, 135103, doi:10.1088/0022-3727/49/13/135103 (2016).
4. Fuks, M. I. & Schamiloglu, E. 70% efficient relativistic magnetron with axial extraction of radiation through a horn antenna. *IEEE Trans. Plasma Sci.* **38**, 1302–1312, doi:10.1109/TPS.2010.2042823 (2010).
5. Liu, M., Fuks, M. I., Schamiloglu, E. & Liu, C. Operation characteristics of A6 relativistic magnetron using single-stepped vavities with axial extraction. *IEEE Trans. Plasma Sci.* **42**, 3344–3348, doi:10.1109/TPS.2014.2352353 (2014).
6. Liu, M., Liu, C., Fuks, M. I. & Schamiloglu, E. Operation characteristics of 12-cavity relativistic magnetron with single-stepped cavities. *IEEE Trans. Plasma Sci.* **42**, 3283–3287, doi:10.1109/TPS.2014.2311458 (2014).
7. Liu, M., Fuks, M. I., Schamiloglu, E. & Liu, C. Frequency switching in a 12-cavity relativistic magnetron with axial extraction of radiation. *IEEE Trans. Plasma Sci.* **40**, 1569–1574, doi:10.1109/TPS.2012.2196291 (2012).
8. Li, T., Li, J. & Hu, B. Studies of the frequency-agile relativistic magnetron. *IEEE Trans. Plasma Sci.* **40**, 1344–1349, doi:10.1109/TPS.2012.2189025 (2012).
9. Shi, D.-F., Qian, B.-L., Wang, H.-G., Li, W. & Wang, Y.–W. A compact mode conversion configuration in relativistic magnetron with a TE_{10} output mode. *IEEE Trans. Plasma Sci.* **43**, 3512–3516, doi:10.1109/TPS.2015.2433731 (2015).
10. Hoff, B. W., Greenwood, A. D., Mardahl, P. J. & Haworth, M. D. All cavity-magnetron axial extraction technique. *IEEE Trans. Plasma Sci.* **40**, 3046–3051, doi:10.1109/TPS.2012.2217758 (2012).
11. Shi, D.-F., Qian, B.-L., Wang, H.-G., Li, W. & Du, G.-X. A novel relativistic magnetron with circularly polarized TE_{11} coaxial waveguide mode. *J. Phys. D: Appl. Phys.* **49**, 465104, doi:10.1088/0022-3727/49/46/465104 (2016).
12. Uhm, H. S. A kinetic theory of the extraordinarymode perturbations in cylindrical relativistic magnetrons. *Phys. Fluids B* **4**, 740–749, doi:10.1063/1.860217 (1992).
13. Balk, M. C. 3D magnetron simulation with CST studio suite. *Proc. IEEE Int. Vacuum. Electronics Conf.* (*Bangalore, India, 21–24 February 2011*) (Piscataway, NJ: IEEE) pp. 443–444 (2011).
14. Zhou, J., Liu, D., Liao, C. & Li, Z. CHIPIC: an efficient code for electromagnetic PIC modeling and simulation. *IEEE Trans. Plasma Sci.* **37**, 2002–2011, doi:10.1109/TPS.2009.2026477 (2009).

Acknowledgements

This work was supported by the National Natural Science Foundation of China (Grant No. 51377164).

Author Contributions

Di-Fu Shi conceived and designed the RM. Di-Fu Shi and Bao-Liang Qian performed the theoretical analysis of mode excitation. Di-Fu Shi performed the cold and hot simulation verifications. Hong-Gang Wang, Wei Li and Guang-Xing Du provided guidance and assistance on PIC simulations. Di-Fu Shi and Bao-Liang Qian wrote the manuscript.

Additional Information

Competing Interests: The authors declare that they have no competing interests.

Publisher's note: Springer Nature remains neutral with regard to jurisdictional claims in published maps and institutional affiliations.

Open Access This article is licensed under a Creative Commons Attribution 4.0 International License, which permits use, sharing, adaptation, distribution and reproduction in any medium or format, as long as you give appropriate credit to the original author(s) and the source, provide a link to the Creative Commons license, and indicate if changes were made. The images or other third party material in this article are included in the article's Creative Commons license, unless indicated otherwise in a credit line to the material. If material is not included in the article's Creative Commons license and your intended use is not permitted by statutory regulation or exceeds the permitted use, you will need to obtain permission directly from the copyright holder. To view a copy of this license, visit http://creativecommons.org/licenses/by/4.0/.

© The Author(s) 2017